LABORATORI NAZIONALI DI FRASCATI
SIS – Pubblicazioni

LNF–96/028 (P)
18 Giugno 1996

Commissioning and Operating Experience with the LISA Superconducting Accelerator

M. Castellano, L. Catani[#], M. Ferrario, S. Kulinski[$], M. Minestrini, P. Patteri, S. Tazzari[#], F. Tazzioli

INFN – Laboratori Nazionali di Frascati, P.O. Box 13, I–00044 Frascati (Italy)

[#] INFN – Sezione di Roma II and Università di Roma Tor Vergata – Italy

[$] Soltan Institute for Nuclear Studies – Swierk – Poland

Abstract

The commissioning of the LISA superconducting (SC) RF electron linac at INFN Frascati Laboratories has been concluded although, due to a change in program priorities, the full possibilities of the machine have not been exploited.

In this report we illustrate the results achieved so far and the difficulties encountered in commissioning, with the hope that this material might be of some help to those who intend to start the enterprise of building a SC linac in a non specialized environment.

The part concerning the SC system is particularly stressed, but a relevant attention is also devoted to the traditional room temperature injector, the proper setting of which is fundamental to achieving the high beam quality that such a machine allows.

PACS.; 29.15.Dt

Submitted to Nucl. Instr. & Meth. A

1 – Introduction

The INFN Frascati National Laboratories (LNF) started the LISA project, concerning the construction of a superconducting (SC) radiofrequency (RF) linac [1], in 1988, in the mainframe of an effort by the Laboratory to promote activities in the field of SC–RF technology applied to accelerators.

At the time a revival of interest in the technology of SC RF had started in the wake of the work being done at CERN and KEK to raise the energy of existing large circular colliders (LEP and Tristan), and of the start of the CEBAF project of a SC CW machine for nuclear Physics, for which purposes the fields then achieveable (3 to 5 MV/m) were amply adequate.

Although efforts had begun to increase the achievable gradients, having in view the application to linear colliders, both for the realization of high luminosity flavour factories at intermediate energy level [2] and for pushing the threshold of electron colliders into the TeV range, because LISA was conceived as a test and training facility to be operational in the shortest possible time, its field level was specified to be 5 MV/m.

LISA was designed for a maximum energy of 25 MeV and a beam current, averaged on a pulse duration of several milliseconds, of 2 mA. The repetition rate was determined by the restriction on the average beam power to stay below 1 kW for radiation safety reasons. Its main characteristics are reported in Table I. The choice of the frequency was the subject of much debate. A frequency of 500 MHz, towards the low end of then proven designs was chosen as a compromise between minimum possible beam loading effects and size [3]. Today and for the same kind of application, one would probably tend to choose a higher frequency, in the L–band.

Table I– Parameters of LISA.

Energy	25 [MeV]
Bunch length	2.5 [mm]
Peak current	5 [A]
Duty cycle	<2 %
Average macropulse current	2 [mA]
Invariant emittance	10^{-5} [πmrad]
Energy spread (@25 MeV)	$2\ 10^{-3}$
Micropulse frequency	50 [MHz]
Macropulse frequency	10 [Hz]

The choice of beam parameters was dominated by the idea of using the machine as a driver for a high power FEL in the infrared radiation region [3], an application for which the intrinsically high beam quality and long duty factor of a SC accelerator seemed ideally suited. The interest of such an application has been later confirmed by the start of several other similar projects in Europe, the USA and Japan (CLIO, CEBAF, JAERI, etc)

The original design therefore included a 25 MeV transport channel to take the beam through an undulator and the associated optical cavity. A recirculation loop was also foreseen to

investigate the possibility of recovering part of the beam energy after its interaction with the radiation field, to increase the efficiency of the FEL.

An infrared FEL was at the time also of great interest as an advanced synchrotron light source, to complement the equipment of the SR Laboratory active at LNF around the ADONE storage ring. FEL operation would also provide the best diagnostic tools to optimise the accelerator performance.

At the beginning of the '90s however INFN decided the construction of the DAPHNE Phi– factory to become the first priority of the Laboratory, thereby moving SR activities and the LISA project to a lower priority level and eventually cancelling its FEL part. The construction of the machine, started at the end of 1989, was nevertheless completed in 1993.

In the following, a short description of the accelerator is given and its commissioning described, with enphasis on beam diagnostics and on the performance of the SC accelerating structure.

2 – General layout

The philosophy underlying the choice of the machine configuration was to adopt a traditional design for the injector and a proven one for the SC cavities, thus concentrating the research efforts on the obtainment of a high brightness beam and on the problems of operation of a SC linac.

The accelerator main components are:

– a 1.1 MeV, room temperature, injector with a thermionic gun and a high duty cycle beta–graded capture section,
– an achromatic, isochonous, 180 degree bend,
– four, 1.2 m long, 500 MHz SC accelerating cavities, each giving 6 MeV.

Two energy analysing magnetic spectromers are also provided at the 1.1 MeV and 25 MeV levels.

Each cavity is contained in a separate cryostat, for flexibility of operation, at the expense of cryogenic efficiency. The cavities are four–cell bulk Niobium structures, cooled at 4.5 K by a closed loop refrigerator. The design of the cavities and of their accessories (coupler, HOM suppressors, etc.) is based on the proven DESY cavities for HERA [4]. The layout of the accelerator is shown in Figure 1; transport lines and cavity for FEL operation, designed and partly built, are not shown.

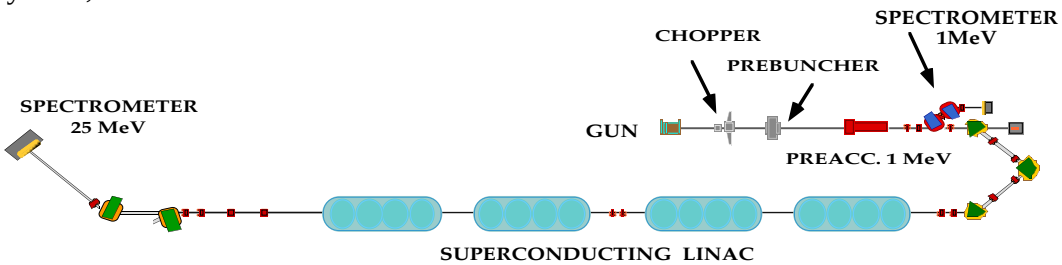

Figure 1– Layout of LISA.

The machine is housed in an underground vault with 1 m thick concrete walls. RF and magnet power supplies, the refrigerator cold box and the control room are all at ground level.

Low level RF systems and vacuum power supplies are housed in the control room. A special housing on separate foundations is provided for the refrigerator compressor, at a distance of about 80 m from the accelerator, to minimise transmission of vibrations.

The machine was designed for continuous beam operation and, given also its size, power consumption was not a serious constraint. All power supplies and generators are CW and the actual pulsed beam structure, a fall–back mode of operation at present used, is obtained by low level modulation. The wall plug to beam peak power efficiency is thus a low figure of 7%. Normal power consumption is about 0.7 MW, of which 0.3 MW for the refrigerator, 0.2 MW for the RF and the rest for water cooling, magnets and controls.

An overall view of the accelerator is shown in Fig. 2.

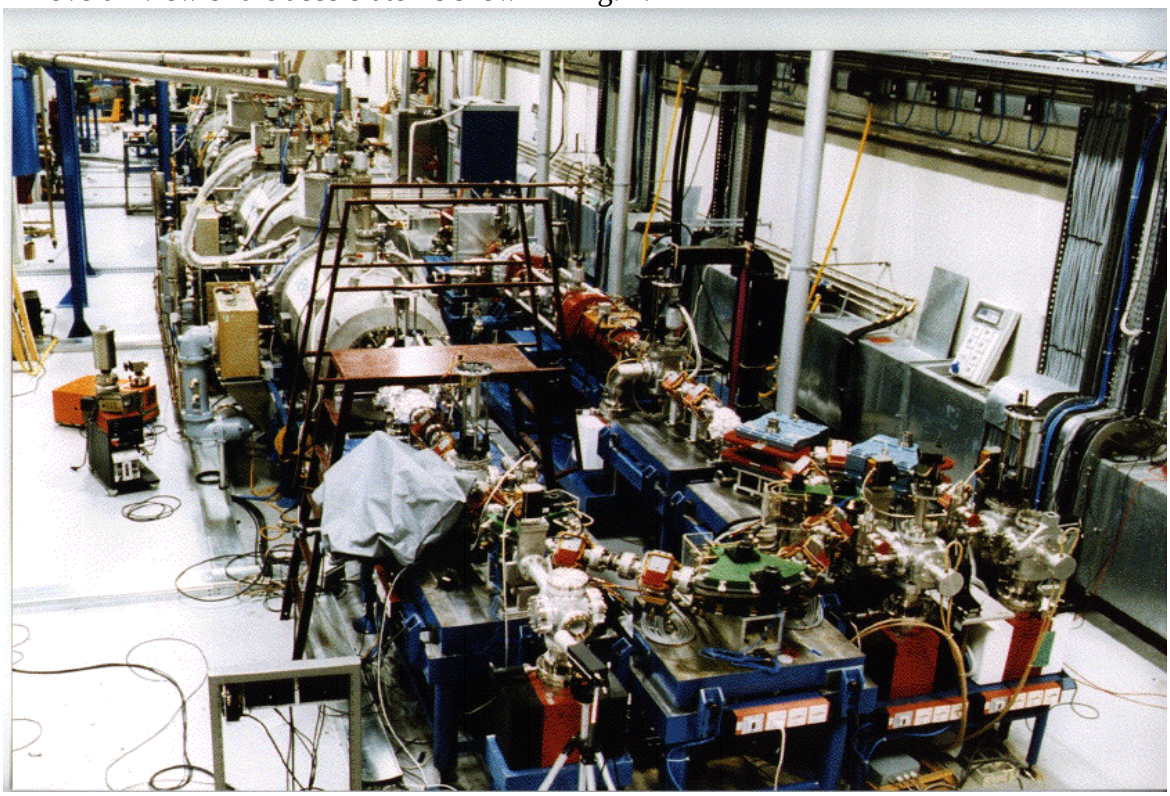

Figure 2 – View of the accelerator.

3 – Beam Optics

The beam optics design was guided by the requirements of the FEL application. In particular the dependance of the optical gain from the electron peak current and the length of the optical cavity have led us to reduce the microbunch frequency to 50 MHz keeping constant the average current of 2 mA. Much care has then been given to obtain, and preserve, the minimum bunch length. The optics of the injector have been designed with two programs, LISA [5] and PARMELA [6]. The first one calculates the relativistic axial dynamics (without space charge) of particles in the various elements of the system and allows some optimization. Two parameters were optimized: the bunching parameter B and the axial electric field in the capture section. The preliminary design was made with LISA and then checked with PARMELA, in a version that accepts an analytical expression of specified electric and magnetic fields. Transverse envelope, bunch length and emittance along the injection system are reported in [6].

The longitudinal phase space is affected by the space charge force, so the bunch length at

the entrance of the capture section must be kept above the minimum one achievable with the prebuncher, to contain the emittance blow–up produced by the current density increase. The bunch phase extension at the entrance is 40^{o} or 7 mm (at 2500 MHz). According to PARMELA all the beam is accepted in the section and at its output 85% of the initial currrent is contained in $\approx 6^{o}$ i.e. 2 mm while the remaining portion is distributed in long tails.

The 180° bending arc optics is designed to be achromatic and isocronous, taking into account also the variation of electron velocity with energy, still noticeable at 1.1 MeV [7].

The setting of the quadrupoles between the magnets is strongly constrained by this condition, so two DFD quadrupole triplets were used at the entrance and exit of the 180° bending arc. This choice would easily allow beam matching from the capture section to the arc in spite of large difference between the calculated and real exit optical functions. Before the last quadrupole upstream the arc a pulsed magnet steers the beam toward the injector spectrometer line.

Actually, the solenoidal field of the capture section had to be lowered with respect to the nominal one to avoid multipacting discharges, while the downstream quadrupole strength had to be nearly doubled to improve the transport efficiency in the arc. In fact the beam Twiss parameters at the exit from the capture section, as deduced from the emittance measurements, have resulted different from those of computer simulations, may be due to asymmetries introduced by deflections.

The same cautelative considerations suggested to have four quadrupoles at the exit of the SC linac to ease the critical matching to the 25 MeV arc guiding the beam to the undulator. Tight constraints on its transfer matrix were imposed by the requirement of beam quality preservation for the FEL experiment [8]. The line section which serves both the arc and the spectrometer uses the same setting, up to first magnet of the arc. The sc linac line is made of two sections, each comprising two cavities, joined by drifts of $\beta\lambda$ length. Between the two sections a quadrupole doublet ensures transverse focusing. The steering coils on the yokes of these quadrupoles have played an essential role in correcting a strong deflection impressed on the beam by the first cavity group. This may be due to an internal disalignment of the electromagnetic axis of the cavities, as the eventual kicks imparted by the main couplers should be balanced by the alternate left–right input configuration adopted.

The quadrupoles and the magnets for the 1 MeV arc were designed and realized in the LNF; the magnets for the 1 MV spectrometer, which had to be laminated magnets due to pulsed operating mode, were realized by a specialized firm.

In the design of the lines at the exit of the SC linac just one type of quadrupole and of magnet was used avoiding, for economical reason, very specialized design. Their specifications were optimized for the three achromatic doublets composing the arc choosing a wedge angle of 5° on both faces The spectrometer magnet uses one of these magnets at higher field to provide 45° deflection; the resulting large wedge angles ensure vertical focusing even without downstream quadrupoles. The dispersion $\Delta x = \eta\ \Delta E/E$ at distance L_s is therefore simply $\eta' L_s\ \Delta E/E = \tan(45°)\ L_s\ \Delta E/E \rightarrow 4\ 10^{-4}$ /mm. The horizontal size of the beam at the focal plane of the spectrometer is ≤ 1 mm at the nominal emittance. In the range of expected energy spread $\approx 2\ 10^{-3}$ the spectrometer resolution is still useful even if ε_n were one order of magnitude worse than the nominal one.

The steering system uses different types of coils along the machine.

In the 100 keV line air–wound coils are used to avoid even small hysteresis effect due to an iron core. Compensation of the Earth's magnetic field with long coils was useful in the early stage of the commissioning, but it was later given up because the iron parts yokes of the solenids and stands did not allow a uniform cancellation of the Earth's field; localized steering coils provided more flexible correction system.

Steering fields in the 1.1 MeV line are obtained by auxiliary windings around the yokes of the quadrupoles; in this way, since the beam position monitors are housed in the quadrupole bores, the trajectory correctors act in the same place where the beam displacement is measured.

A compensation coil around the first magnet of the spectrometer is used to cancel the residual field.

Table II – Parameters of the magnetic elements.

Bending magnets	**deflecting angle**	**nom field Gauss**	**wedge angle**
1 MeV arc #1, #3	45°	200	
1 MeV arc #2	90°	200	
1 MeV spectrometer #1, #2	60°	200	
25 MeV arc #1	30°	1667	5°
25 MeV spectrometer #1	45°		12.5°

Focusing magnets	**#**	**max field**	**kmax [m^–2]**	**length [m]**
Solenoid	8	500		0.1
1 MeV quad	14		60	0.1
25 MeV quad	5		30	0.2

The steering magnets after the SC linac are air–wound coils placed around the BPM's; in this line the quadrupoles cannot house BPM inside, because of the smaller bore required to reach the design gradient.

The parameters of the magnetic elements used along the accelerator are summarized in Table II.

4 – Machine hardware and vacuum

The vacuum specifications for linac operation are usually more relaxed than for a storage ring; however in LISA two peculiar features had to be taken into account: potential harmfulness of low vacuum for the sc cavities and high average beam power, which could cause strong gas desorption and even activation of serviceable parts hit by the beam. Therefore the hardware and vacuum system of LISA were designed to satisfy more tight constraints. Distribuited ion pumping ensures pressure lower than 1 10^{-8} mbar all along the machine; in the straight section at the entrance and exit of the sc cavity string pumping speed is larger, to get a residual pressure < 2 10–9 mbar; the pumping speed and molecular conductance in the 25 MeV spectrometer and

beam dump were calculated to ensure a pressure rise < 1 10–9 mbar at the sc linac when pressure in the beam dump, 7 m downstream the exit of the last cryostat, rises up to 1 10–6 mbar. Extensive usage of aluminium, instead of stainless steel, was made in the construction of the vacuum chamber to counteract the danger of activation.

5 – The Injector

The choice of the injector energy, 1.1 MeV, is a compromise between the need to inject a fully relativistic beam into the SC cavities and the cost of the system. Parameters other that the energy were mostly determined by the FEL application.

A traditional, room temperature design was adopted to stay with proven Laboratory technology and to have a compact capture section, surrounded by a magnetic solenoid providing efficient focusing in the presence of strong space charge forces.

The main beam characteristics are listed in Table III.

Table III – Beam characteristics.

Energy (MeV)	1.1		
Average current (mA)	2	Bunch rep.rate (MHz)	≈ 50
Peak current (A)	5	Bunch length (ps)	6÷10
Macropulse duration (ms)	2 –> CW	Normalized emittance (m·rad)	10^{-5} π
Duty cycle		Energy spread	< 1%

The injector layout includes a 100 keV thermionic gun followed by two choppers, one at the 10th subharmonic (50 MHz) and the other at the fundamental frequency f_0 = 500 MHz, a prebuncher at f_0 and a 1 MeV, 5th harmonic (2.5 GHz), beta graded capture section. Focusing solenoids, steering coils, collimators and diagnostic elements are distributed along the line as sketched in Fig.3.

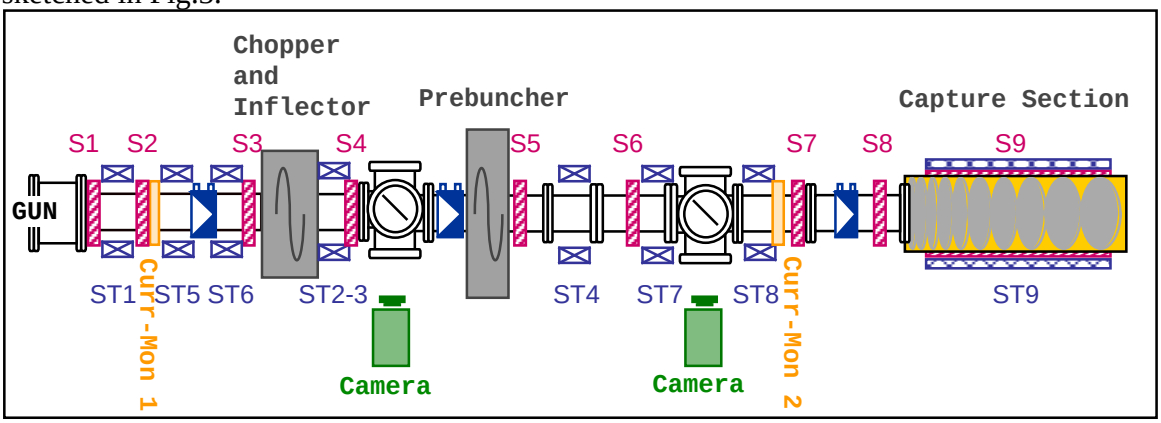

Figure 3 – Injector line.

The gun is of the Pierce geometry, thermionic, triode type[9]. Its measured emittance vs. current is shown in Fig. 4. The spherically shaped cathode (diameter = 6.4 mm, curvature radius 40 mm) is of the dispenser type.

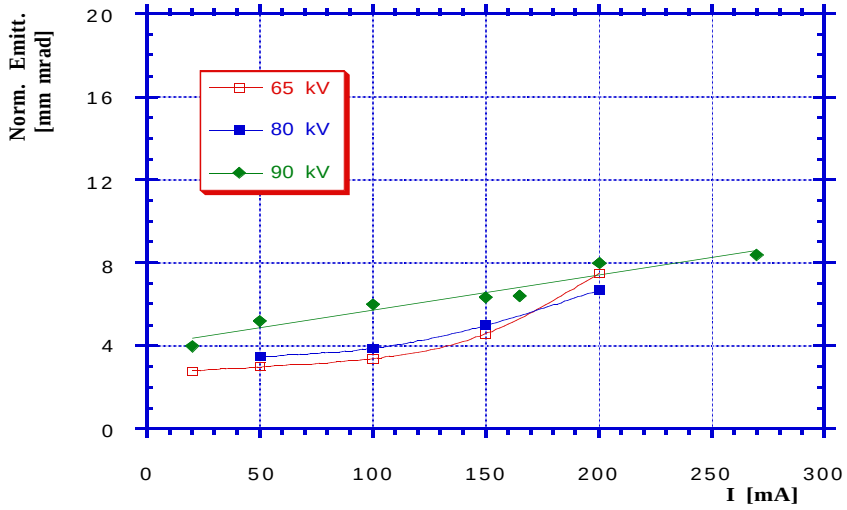

Figure 4 – Gun emittance vs. current.

The performance of the gun has been checked off line [10]. The design had been optimized for a larger current than the one subsequently used in the machine (≈ 150–200 mA), thus the emittance at this current has resulted larger than that obtainable with a cathode of smaller area corresponding to these currents. Nevertheless the measured emittance value of (0.4–0.8)x10–5 π m rads is still slightly smaller than the designed value. Another inconveneience due to the smaller current is that the waist position, being too close to the cathode, is less favourable for subsequent focusing.

The subharmonic chopper (inflector) consists of a pair of deflecting electrodes. It has the function of selecting one bunch over ten. The main chopper is a RF cavity operated in the TE_{102} deflecting mode at the main frequency ≈500 MHz. It works in combination with a collimator and is followed by a couple of steering coils to compensate the imparted angle. The chopping is performed on the crest of the sine wave by superposing a bias voltage on one of the electrodes of the inflector and by a proper choice of the steering fields. Thus one also obtains the least degradation of the beam emittance.

The prebuncher is a TM_{010} mode cavity with reentrant nose cones, working at the same frequency as the SC cavities, the parameters of which are shown in Table IV.

Table IV – Prebuncher parameters.

Frequency	≈500 MHz
Gap length	6 cm
Voltage	V=9.5–11.5 kV
Drift space	D=1.36 m
Phase compression	25–33
Bunching parameter	B=1.45–1.5

The bunching parameter is defined as $B= \pi DV/V_g \lambda ß$, where Vg is the gun voltage, ß the corresponding relative velocity, λ the wavelength in the prebuncher. The phase compression is very sensitive to B and therefore V and Vg must be stabilized within 1%.

The capture section is a normal conducting, S–band, standing wave, biperiodic π/2, β–graded accelerator, working at the 5th harmonic of the basic frequency (≈ 2500 MHz). It is designed to work in principle in CW mode with power dissipation of 20 kW/m. An axial magnetic field produced by superimposed solenoids counterbalances the radial defocusing forces due to space charge or RF fields. The magnetic field varies along the section, with a peak at the entrance about twice the average value.The section has been designed and built at the Swierk Zoltan INS. The main parameters of the section are given in Table V.

Table V – Capture section characteristics.

Frequency	≈2500 MHz
Avg accelerating field	1 MV/m
Input ß	0.54
Output ß	0.94
Length	1.1 m
Number of cells	23
Peak power input	30 kW

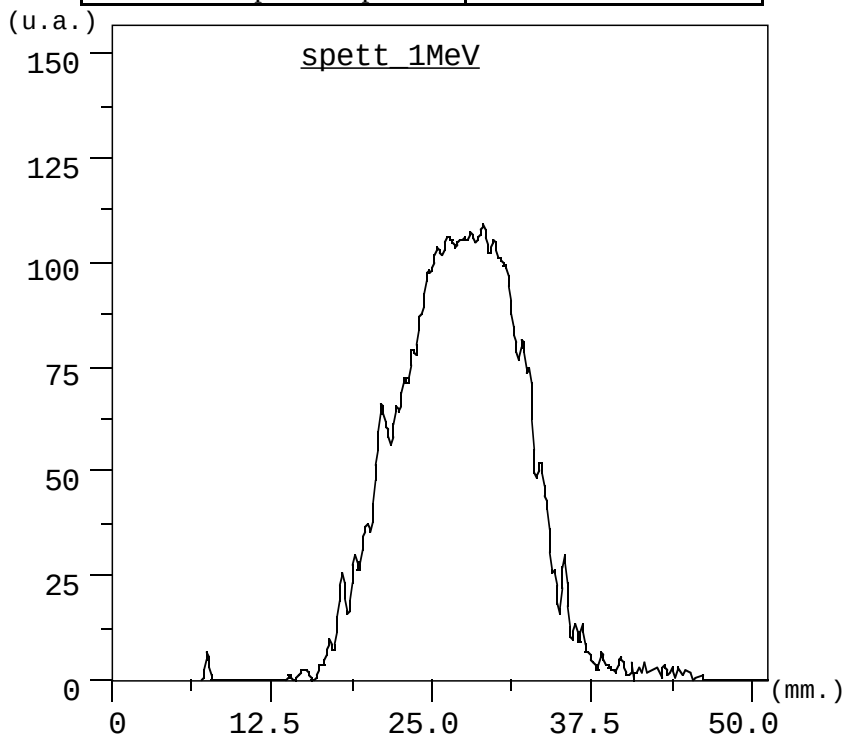

Figure 5 – Energy spectrum of 1 MeV beam; $\partial E/E=5x10^{-3}\partial x$(cm).

The energy spectrum of the beam after the capture section has been measured with the magnet spectrometer and is shown in Figure 5.

The emittance of the 1.1 MeV beam has been measured by fitting the curve of variation of the dimension of the beam image on a target with the focusing strength of a preceding quadrupole. The result depends on the strength of the field of the solenoid superimposed on the capture section and is 8 π mm mrads at 800 Gauss.

Current transmission efficiency through the capture section is not full. Usually we require about 3 mA at the entrance to obtain 2 mA at the exit within 1% energy bin. This may be due both to unperfect chopping ahead of te section and to transverse losses in the section itself due to trajectory inclination at the entrance. In fact the measured emittance at the exit has been found to be remarkably less than expected, showing that part of the beam is scraped off by the irises.

Numerical calculations have shown that the peak current Ip, which is inversely proportional to the bunch length at the end of the capture section is a very sensitive function of the bunching parameter and has a rather sharp maximum for B=1.45. To be close to the maximum of Ip, variations of the B should be smaller than 0.5%. It means that changes of both prebuncher and gun voltages should be smaller than 0.5%. Prebuncher phase changes also must be kept below a few degrees.

Experimentally the proper choice of the optimum values of voltages and phases were found by measuring the current after the 1 MeV capture section and searching for its maximum. It was also helpful to look for the maximum of beam loading voltage clearly seen on the reflected RF pulse from the capture section. Since the pulse length of Lisa can be of the order of a few milliseconds, it is very important that the variations of gun and prebuncher voltages during the pulse be kept below 0.5%. The effect of such changes was observed experimentally when a part of the bank of charging capacitors in the gun power supply was excluded, producing a voltage droop of 0.5%. This caused a corresponding sag of about 30% of the current after the capture section during the pulse.

The proper setting of the subharmonic inflector, bias and chopper voltages was performed by first transporting the maximum current up to the capture section without bias and RF voltages, then increasing the bias voltage until the current was cut off. Successively the inflector voltage is turned on and bias increased again until the current is cut off. Finally the chopper voltage is turned on and increased until the current reaches the nominal 2 mA value. The prebuncher is then activated and the current accelerated through the capture section.

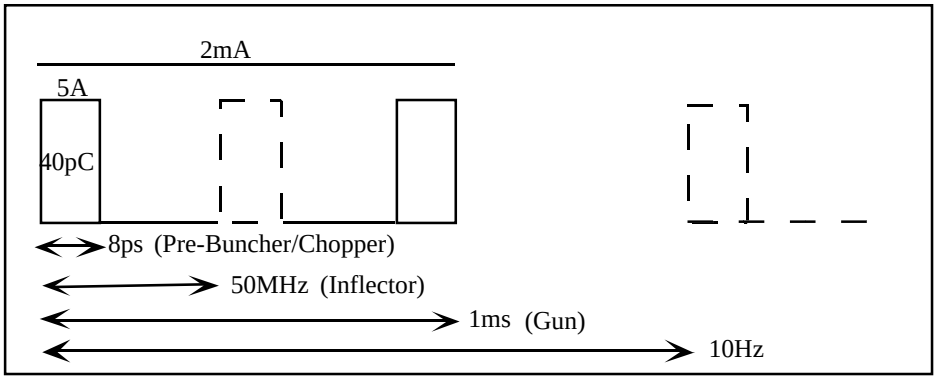

Figure 6 – Beam time structure.

The beam time structure (see Fig. 6) has been checked by recording the frequency spectrum of the voltage induced by the accelerated beam on a strip–line detector downstreem of the capture section. If the parameters are properly set one observes strong sidebands at the inflector 50 MHz frequency around the multiples of the 500 MHz fundamental frequency (Fig. 7). Moreover the ratio between the amplitude of 500 MHz and 2500 MHz lines gives an estimation of the bunch length. Infact if the 2500 MHz line is dominat it means that the bunch

entering the capture section is too long and is captured on more than one rf bucket. If the bunch length is of the order of the acceptance of the capture section (100 ps) the 500 MHz line is dominat. The proper bunch length (10 ps) corresponds to a ratio of the order of one.

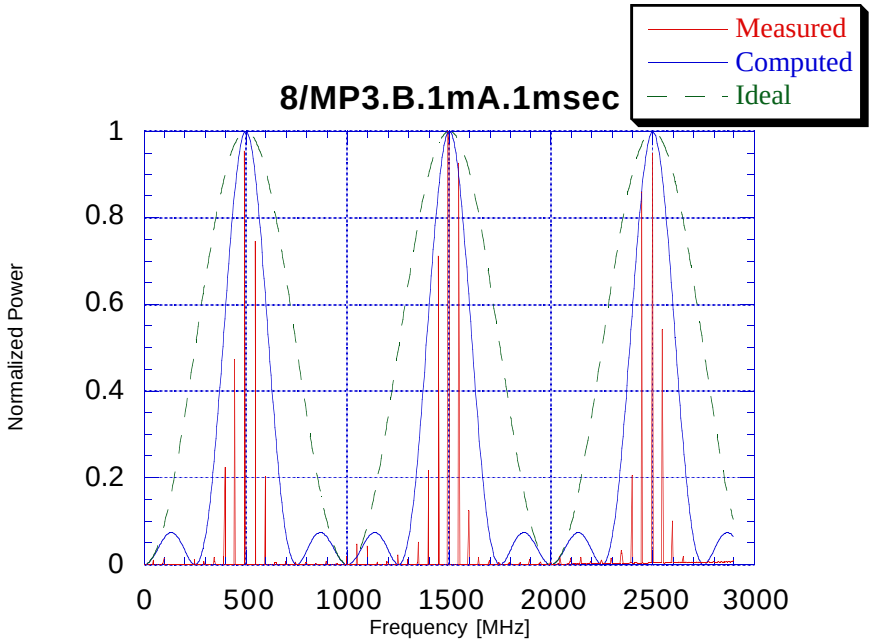

Figure 7 – Measured spectrum lines, computed and ideal envelops.

On the whole, after elimination of some spurious effects (an unterminated deflecting electrode was accumulating beam charge, a mulfunctioning of the gun power supply caused a large voltage sag, etc.) the behaviour of the injector resulted enough predictable according to the design. No compensation of the earth's magnetic field was required, due to the abundance of steering coils. Some trouble is caused by the necessity of frequent readjustments of the phase between prebuncher and capture section to keep a constant current in 1% energy bin. This is only partially due to real phase drifts, as fluctuations of prebuncher and gun voltages have an equivalent effect. Current fluctuations are also caused by cumulative transverse disturbances, especially if the beam trajectory is not kept everywhere very close to the axis. After a good setting of the beam trajectory and other parameters, the residual peak current fluctuation in 1% energy bin is of the order of 20%.

6 – The superconducting cavities

The unit module of the SC linac is a four–cell, bulk Nb, RRR=200, 500 MHz cavity, housed in an individual cryostat and operating at 4.2 °K. The acceleration length is 1.2 m, while the overall module length is 2.5m. The R/Q geometrical impedance is 460 Ω.

Besides the main power coupler, the cavity is equipped with a pick–up probe for field sampling and three higher order mode suppressors (HOM), one for TM and two for TE field modes.

It has a slow mechanical tuning system by elastic variation of the cavity length. A sketch of the module section is shown in Fig. 8 The volume of the LHe container is partially filled with Al bodies, to reduce the amount of LHe for safety reasons, at the expense of a longer cooling

time. The modules have been designed, on the basis of the original DESY Hera design [3], built and tested by SIEMENS–INTERATOM, now ACCEL.

The choice of the frequency was motivated by the reduction of HOM impedances with increasing iris aperture [3]. This factor is most relevant to colliders and to very high power FELs operating at very high micro–bunch charges. In LISA, because beam spectrum frequency lines do not overlap higher order cavity resonances appreciably, single–bunch HOM wakefields are negligible and resonant multibunch effects are very small. In fact we have been able to operate at or near nominal current without terminating the suppressor ports.

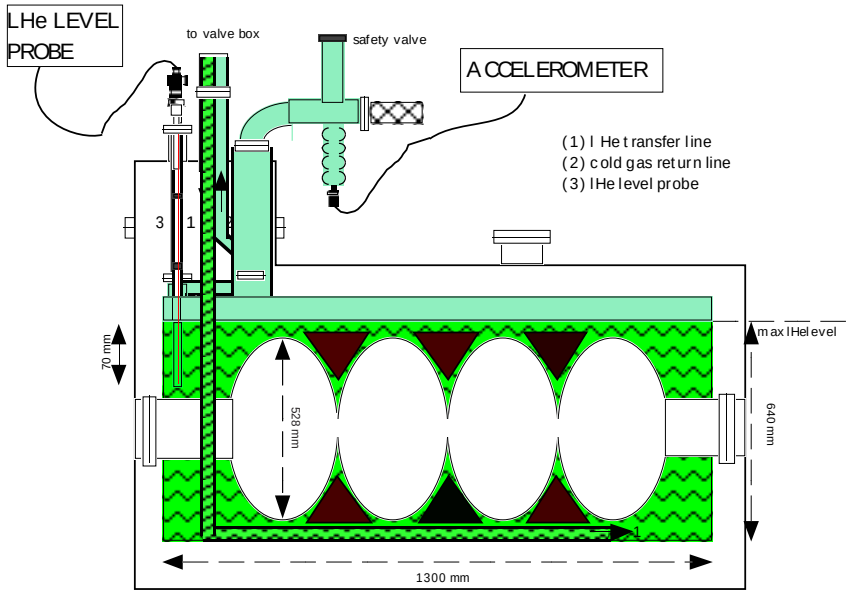

Figure 8 – Sketch of the SC accelerating module.

The main cavity parameters, such as external quality factor of the main coupler, Q_e,and of the field pick–up, Q_a, and the unloaded quality factor, Q_O, have been first measured at the factory and then re–checked in Frascati.

Figures for Q_a have been obtained from the scattering matrix parameters measured with a spectrum analyzer[11], both at room temperature and at LHe temperature. Some discrepancies have been found between the values measured at the factory and in Frascati on cold cavities. They are explained by the fact that factory measurements on cold cavities were affected by a systematic error caused by fluctuations of the cavity resonant frequency – due to microphonics – that, when the frequency sweep is too fast, smoothed and altered the shape of the resonance curve. The values obtained in Frascati, later confirmed by beam energy measurements with the magnetic spectrometer, are shown in Table VI.

Table VI – Main coupler and pick–up external quality factors.

	Cav#1	**Cav#2**	**Cav#3**	**Cav#4**
Main coupler: $Q_e.10^{-6}$	4.6	8.0	5.1	5.0
Pick–up: $Q_e \cdot 10^{-11}$	2.6	0.6	0.9	3.0

A new method has been devised to measure Q_0 calorimetrically, on line with the refrigerator [11]. This turns out to be important to control the performance and the stability of the machine, and can only be done calorimetrically unless the cavity is equipped with a variable coupler.

The cavity quality factor can be evaluated by simply turning on the RF once the input LHe flow is in fixed equilibrium with the static losses and measuring the resulting level rate of descent. In practice, using the heating resistors, we first introduce into the cryostat a well known amount of power, much larger than that corresponding to static losses, switch the refrigerator to automatic and wait until an (average, imperfect) equilibrium state is reached. Under such conditions the LHe inlet valve setting performs small oscillations around its average position: once the latter position has been determined, the valve is blocked there manually. The fixed LHe input then almost exactly compensates the overall heat input and the level remains sufficiently constant for a rather long time (order of tens of minutes). We can then switch on the RF and measure the liquid level fall rate, only due to cavity wall losses P_C. Measurements can be performed at different RF peak power levels under almost identical experimental conditions, by pulsing the radiofrequency and varying the duty cycle in such a way as to keep the average RF power constant.

Fig. 9 shows a sample of data taken with this technique on the cavity n.1. The RF power corresponds to an accelerating field of 2.8 MV/m; it was switched–on after an equilibrium state had been reached with 30 W of heat added to the static losses. The RF duty cycle was 25% (one 200 ms pulse every 800 ms). The corresponding evaporation rate was 1.91 liters/min.

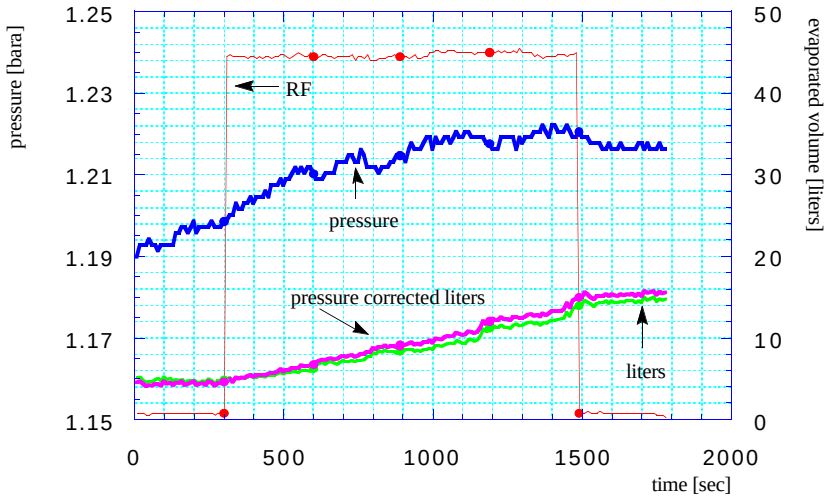

Figure 9 – RF power on : behaviour of the pressure and liquid level vs. time.

In Fig.10 we show the Frascati measurements of Q_0 vs. accelerating field, E, for one of the cavities (the behaviour of the others is similar), and for comparison, the data from the same cavity measured at the factory.

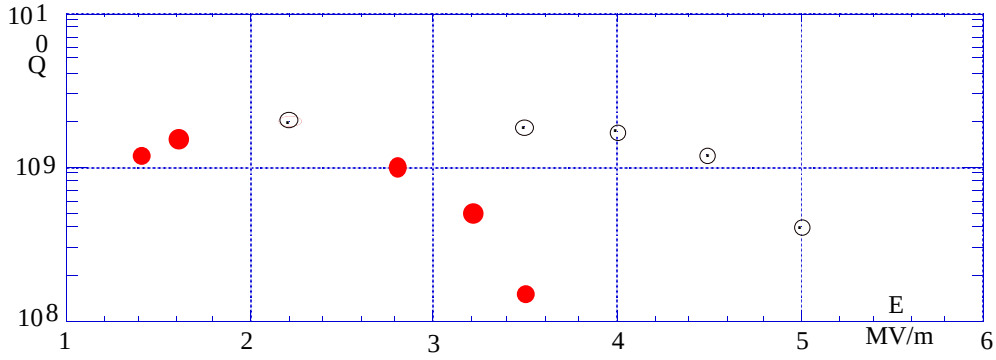

Figure 10 – Q_O vs. accelerating field E @ 4.2 K.

Full dots= Q @ Frascati ; empty dots= Q@ Factory

One can notice that going from factory to accelerator, while at low field Qo is only slightly altered, there is a remarkable lowering of the curve 'knee' (from ~4 to ~3MV/m), to be attributed to field emission as X–ray measurement also show.

This behaviour is most probably to be attributed to some contaminant having migrated to the surface of the cavities from the adjacent parts of the accelerator although the vacuum level next to the cavities, obtained without taking any special precaution during assembly other than those pertaining to a good vacuum practice, is in the range of 10^{-9} mbar.

Even though peak accelerating fields of up to about 6 MV/m, limited by available klystron power and coupling, are obtained in short pulses (0.3 ms), corresponding to a maximum field on the iris of about twice that figure, the peak power turns out not to be sufficient to process away the problem even after lengthy pulsing.

The low field value at which field emission becomes significant prompted us to consider possible field flatness degradation due to alteration of the tune of individual cells in the course of the various successive manipulations of the cavities. A much higher than average field in one of the cells would in fact limit the performance of the whole cavity.

Measurements of field distribution performed at the factory by the usual perturbative method had given a field unflatness figure of ±5%. Because the method could obviously not be applied to cavities in–situ, information on the order of magnitude of the field flatness could only be obtained indirectly from comparing the measured dispersion curve with the theoretical one and with similar measurements performed on known cavities, as explained in the following.

From the definition of coupling constant

$$K = \frac{\nu_\pi^2 - \nu_o^2}{2\nu_o^2}$$

and dispersion relation

$$\nu_\vartheta^2 = \nu_o^2\left(1 + K(1 - \cos\vartheta)\right)$$

eliminating ν_o on the previous equations, we compute the effective coupling constants from measured resonance frequencies with the following relation:

$$K_\vartheta = \frac{\nu_\pi^2 - \nu_\vartheta^2}{2\nu_\vartheta^2 - \nu_\pi^2(1 - \cos\vartheta)} \quad \text{with} \quad \vartheta = \frac{\pi}{4}, \frac{\pi}{2}, \frac{3\pi}{4}.$$

In a well tuned cavity all the K_θ must be equal and hence $\Delta K/<K> = 0$, where $\Delta K = K_\vartheta^{Max} - K_\vartheta^{min}$. On the contrary $\Delta K/<K> \neq 0$ is an approximate indication of the cavity field unflatness.

In Table VII we report coupling constants from measured frequencies of the LISA cavities and for comparison two cases of DESY cavities. With reference to the operating frequency ν_π = 499.798 MHz.

Table VII – Comparison of coupling constants of LISA and Desy cavities.

	CAV–1	CAV–2	CAV–3	CAV–4	DESY NOT TUNED	DESY WELL TUNED
$K_{\pi/4}$	1.91 %	1.87 %	1.98 %	1.91 %	2 %	2.08 %
$K_{\pi/2}$	2.32 %	1.93 %	1.83 %	2.27 %	2.17 %	2.08 %
$K_{3\pi/4}$	3.27 %	1.96 %	1.75 %	3.16 %	2.89 %	2.09 %
$<K_\theta>$	2.5 %	1.91 %	1.85 %	2.45 %	2.35 %	2.08 %
$< K_\theta >$	54 %	4.6 %	12 %	51 %	38 %	0.7 %
E_{min}					1.7	1

As it is reported in previous table Cav. 1 and Cav. 4 reveal a strong deviation from the right tune if compared to the known DESY cases.

7 – The RF System

The principle adopted for the RF system has been to have an independent chain for each element. For small accelerators this is the most efficient solution for phasing and overall voltage stabilization problems.

The 500 MHz signal from the master generator is distributed to the various RF chains through a fan–out system of buffer amplifiers. The 5th harmonic for the capture section is generated by a diode multiplier circuit and the tenth subharmonic for the inflector is generated by frequency division. All power amplifiers are CW and separated from the resonant loads by circulators. Pulse modulation is performed at low level. The RF power to the various elements is shown in Table VIII.

Table VIII – RF power distribution.

	Frequency (MHz)	**Power** (kW)	**Type of device**
Inflector	50	0.25	Solid state
Chopper	500	1	Tetrode
Prebuncher	500	0.3	Tetrode
Capture section	2500	30	Klystron
SC cavity	500	20	Klystron

Each cavity is powered by a separate RF chain equipped with its individual system of feedback loops for the stabilization of voltage, phase and resonant frequency. A typical block diagram of such loops is shown in Fig. 11.

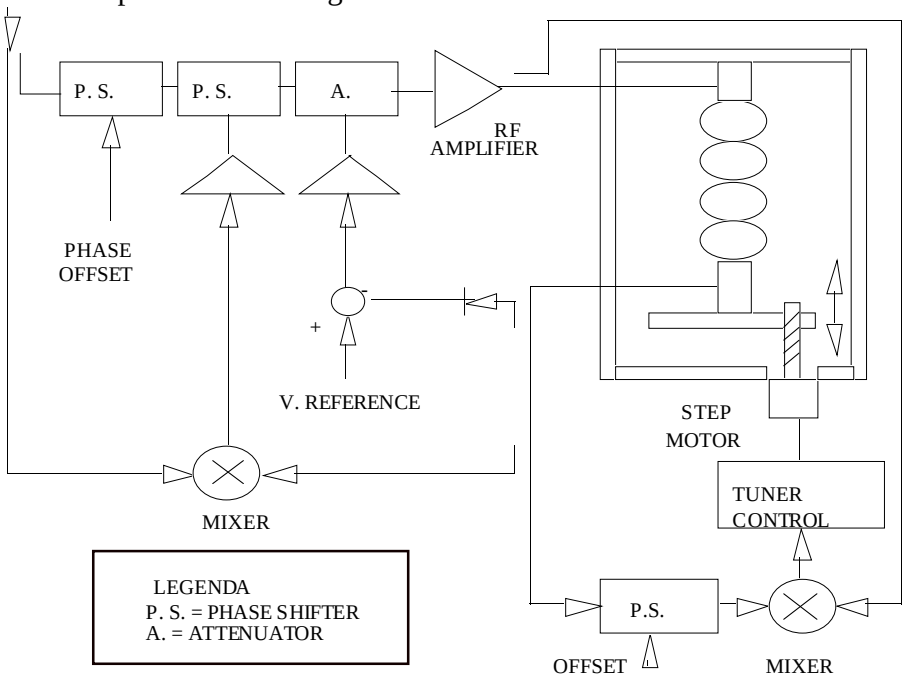

Figure 11 – Stabilization loops : block diagram.

The open loop transfer function is made to approximate a pure integration by cancelling the cavity pole (50 Hz) with a zero and by introducing a very low frequency dominant pole (1 Hz). The Bode diagram of the open–loop transfer function of the amplitude stabilization loop of one of the cavities is shown in Fig. 12.

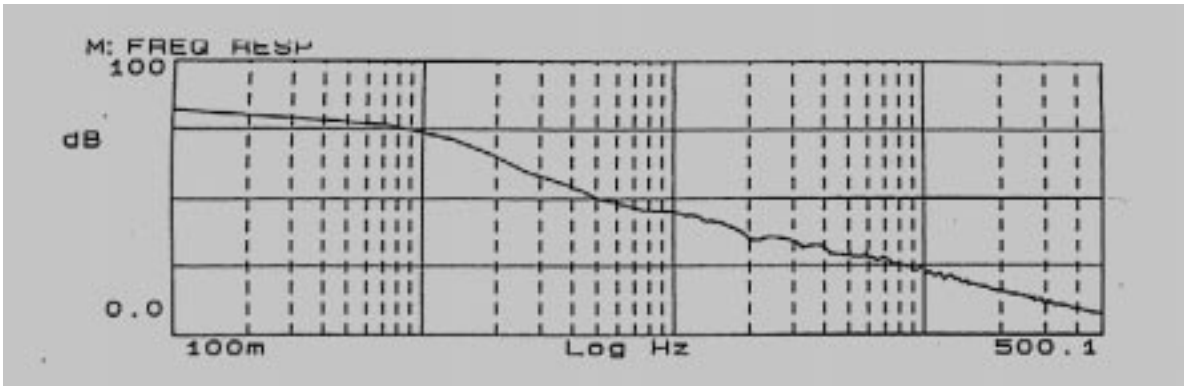

Figure 12 – Bode diagram of the open loop function.

The beam is injected on the flat top of the RF pulse, after the transients have died out. It is to be noted however that the beam itself induces a transient. Fig. 13 shows the dip in accelerating voltage caused by a 2 mA beam current pulse of 1 ms duration when the loop gain is too low; the resulting energy dispersion is very large.

In order to avoid this kind of effect, the beam must be injected on the rising front of the RF pulse, at a time determined by beam loading and by the cavity open loop voltage, so that the positive slope of the voltage waveform compensates the negative one induced by the beam [12].

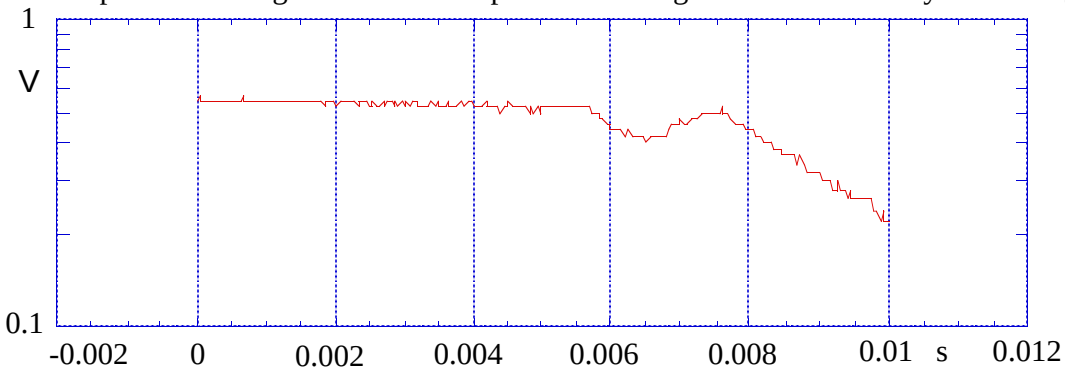

Figure 13 – Transient induced by the beam on the accelerating voltage.

This scheme requires the feedback response on the rising front of the pulse to be linear, a condition not well satisfied by the actual feedback circuit configuration because the final stage of the high gain feedback amplifier is normally saturated when not operating, i.e. in the absence of an RF pulse. When the feedback is gated on, the amplifier must exit saturation before the feedback takes control. This determines an overshoot on the pulse waveshape, and the non linear transient lasts for about 3 ms.

The RF power is not completely switched off in the interval between pulses: a pedestal is kept, sufficient to operate the phase detector that provides the error signal to the slow resonant–frequency tuner.

The design of phase loop is more difficult because of the larger sensitivity of the phase of cavity voltage to frequency deviations. At first the open loop transfer function was chosen similar to the one of the amplitude loop,by approximating it to a pure integration by cancelling the cavity pole (50 Hz) with a zero and by introducing a very low frequency dominant pole

(1 Hz). This configuration was attractive because it allowed a very high static gain. In fact the last operational amplifier, with a resistor–capacitor series on the feedback branch, worked without feedback at low frequencies. This solution did not work in practice because of the excessive excursions of the error signal, which saturated the above said amplifier causing nonlinear distortion and a large time delay.

A simpler configuration was then adopted, with a flat frequency response up to the corner determined by the cavity itself (50 Hz). The static gain was limited to ≈ 200 to avoid loop instability, but it was sufficient to keep phase fluctuations lower tnan 2 degrees.The voltage pulse and the phase error signals of one of the cavities are shown in Figg.14 and 15.

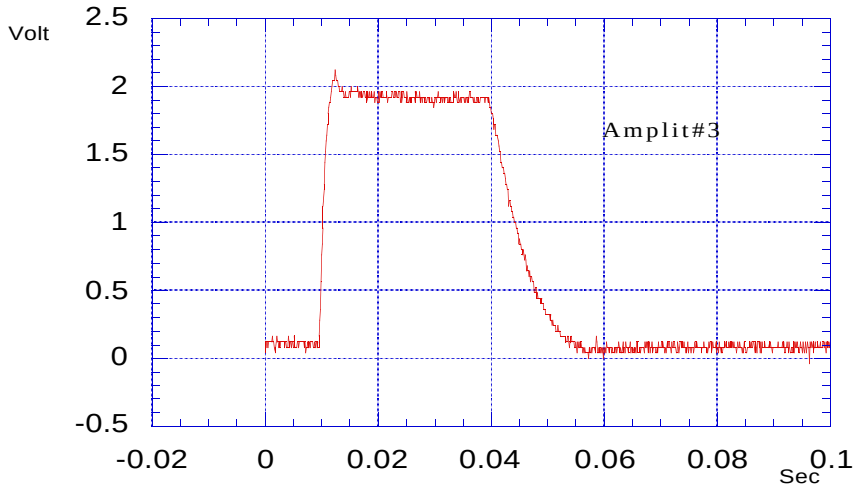

Figure 14 – Typical voltage pulse(1 V=1.5 MV).

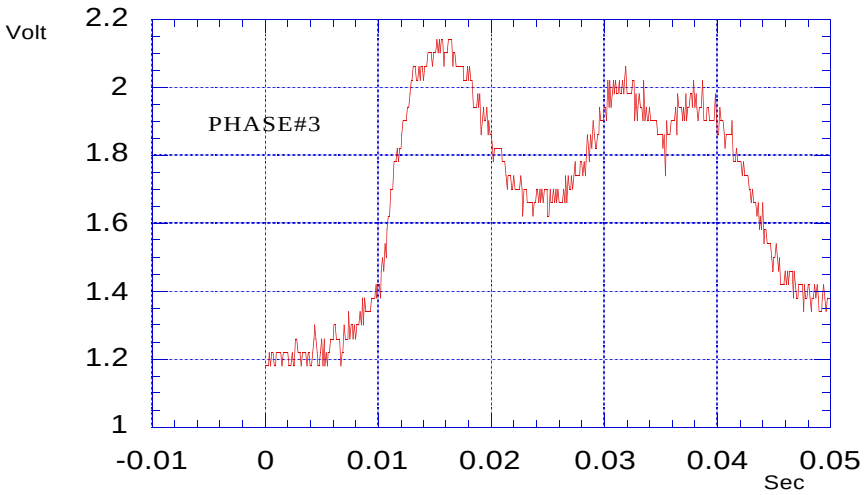

Figure 15 –Typical phase error signal during pulse (1Volt=5 degrees).

8 – The Refrigerator system

The LISA Refrigerator plant is a Sulzer TCF50 Refrigerator able to drive a 300 W load at 4.5 K and 1000 W load at 80 K, with a flow rate of 63.4 g/sec resulting in 7 l/min of LHe flow rate.

A skew Compressor loading Helium gas from a Buffer maintains 13 absolute bar (bara) in the Discharge line and 1.05 bara in the Return line. A special housing on separate foundations is provided for the Refrigerator Compressor, at a distance of about 80 m from the accelerator, to minimize transmission of vibrations.

The high pressure helium enters the Cold Box and is cooled in counterflow with the cold low pressure helium (see Fig. 16). The high pressure stream is split after the first heat exchanger, a part of it (60%) is used for the shield cooling and afterwards is expanded through two turbines to the low pressure line. The remaining high pressure stream (40%) is further cooled in the heat exchangers and then deviated in a By Pass line in order to increase the gas flow rate to the loads, until a temperature (14 K) lower than Helium inversion temperature is reached. Below that temperature the By–Pass line is fully closed and the gas is expanded within two Joule–Thomson valves. In the last JT valve liquefaction partially occurs. The two phase mixture is separated in the LHe dewar where the LHe level is kept constant by a pulsed heat resistor and the vapor returns at low pressure combined with return gas from cryostats, providing the counterflow cooling of the heat exchangers. LHe is distributed from a Valve Box to the 4 cryostats through 4 super insulated Leybold Transfer Lines. The common line from the Cold–Box to the Valve–Box is 24 m long, while the local branches to the cavities are different and have an average length of 4 m.

The LHe level in the cryostats is kept constant by a feedback loop acting on the inlet valve of each cryostat driven by a signal coming from a LHe probe.

Each Cryostat is also equipped with a heat resistor which can be used to increase the thermic load to a certan optimized value for the Refrigerator performance when the cavities are operating at low CW field level or in pulsed mode.

A typical cool down of the whole machine takes 60 hours to reach LHe plus 10 hours to fill the 4 cryostats containing about 100 liters of LHe each. Such a long cooling time is mainly due to the large mass of Alluminium filling bodies in the LHe tank, which reduce the volume of LHe required. The electrical power requirement is 431 KW mainly used to run the compressor motor. The cooling efficiency in then 0.07 % at 4.5 K.

A relevant problem encountered with the cold cavities was the presence of strong vibrations of intrinsic origin, i.e. not transmitted by external rotating machinery or such. The most sensitive method to detect these vibrations is to observe, with a low frequency spectrum analyzer, the output from a phase detector looking at the phase difference between the voltage incident on the cavity and that transmitted at the field pick–up.

A sharp correlation with the spectra of pressure oscillation in the LHe bath has been detected with an accelerometer mounted on a bellow in communication with the LHe tank. A spectrum of pressure oscillation, Fig. 17, showed a peak at a frequency of 30 Hz with an amplitude of 1.5 mbar, associated with a RF phase fluctuations of the order of ± 50 degrees, the exact values being slightly dependent on the status of the refrigerator.

The voltage and phase stabilization loops have a severe task, because the amplitude of the cavity structure vibrations is such as to cause cavity eigenfrequency variations of the order of a half bandwidth (50 Hz). The amplitude loop can cope with the corresponding voltage fluctuations only up to an average cavity voltage of 3 MV, above which the klystron power saturates.

A cross spectrum between cavities shows that the frequency of the line is identical (within 1 Hz bandwidth) for all cavities, indicating that the cause of such vibrations is to be looked for in the interaction of the cryostats with the refrigerator. It could be a thermo–acoustic oscillation somewhere on the Refrigerator lines or a two–phase flow with perturbing gas bubbling.

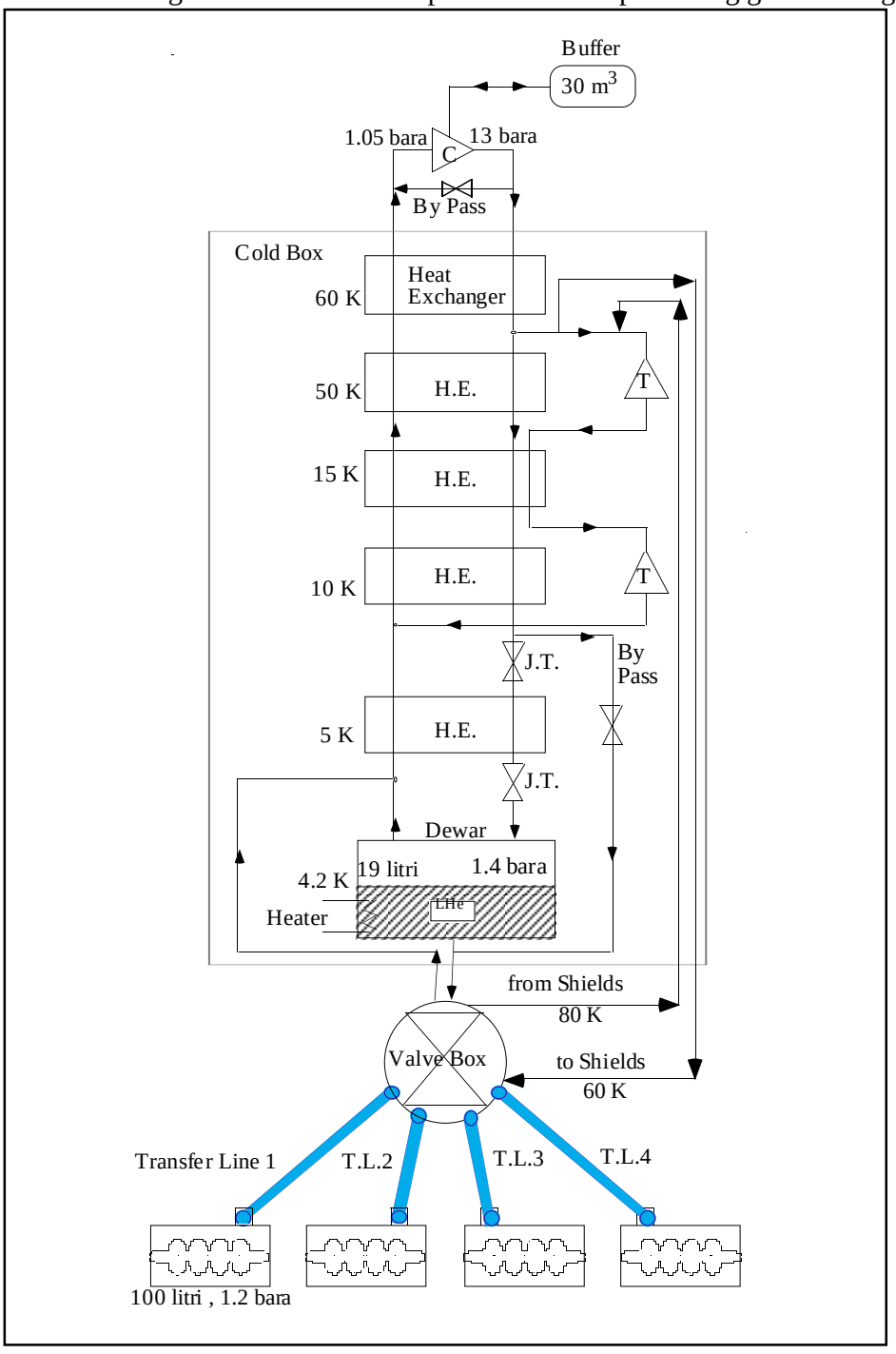

Figure 16 – Sketch of the refrigeration system.

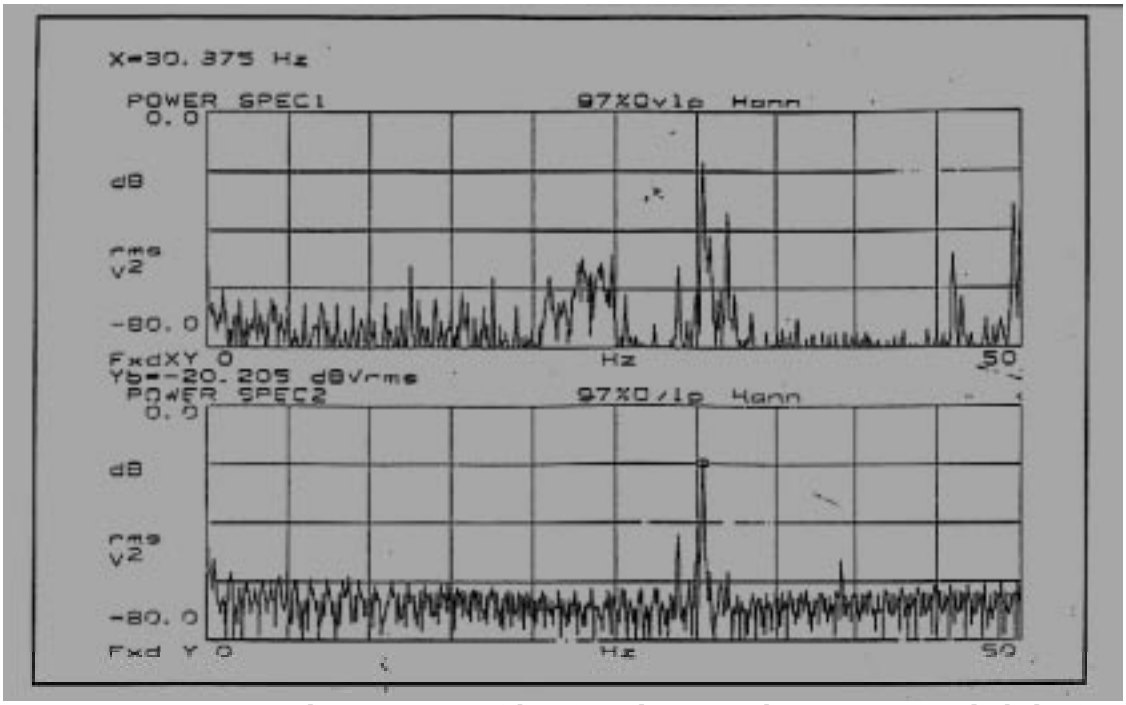

Figure 17 – Helium pressure (above) and cavity phase error signal (below) spectra. Average bath pressure 150 mbar, it shows a peak at 30 Hz frequency with a pressure oscillation amplitude of 1.5 mbar (above) correlated to a cavity rf phase oscillation of $\pm 50^{o}$ (below) at the same frequency.

The first hypothesis is consistent with the line structure of the spectrum. The second one seems to be supported by a dependence of the phenomenon on the pressure drop between cold box and cryostats. Furthermore, it is possible that the vibration is amplified by falling into the bandwidth of a mechanical structure resonance.[13].

The same fenomena have been detected also by other groups and attributed mainly to a pertubation coming from the cryostat inlet LHe line. In fact as in our case when the inlet line goes to the bottom of the cryostat, see Fig. 2, a two–phase LHe flow could induce perturbing gas bubbling in all the bath. A reduction of these perturbations has been obtained, in other laboratories, by cutting the LHe inlet line at the top of the cryostat and filling it as in a "shower" mode (Saclay), or by adding a phase separator dewar on each cryostat (DESY). At CERN a correlation has been found with the LHe level in the cryostat and they succeed to cure oscillations just changing the LHe level working point. Anyway in our case a modification on the cryostat cannot easily be produced because the cryostats cannot be disconnected from each other and accessed.

Many attempts have been done to optimize the Cryostats–Refrigerator interaction in order to reduce pressure fluctuations and to have cavity eigenfrequency variations within the cavity bandwidth. A schematic story of all our efforts is summarized in Table IX with reference to the Cryogenic plant flow chart (Fig. 16).

Increasing pressure in the Suction line together with a decoupling of the Cryostats from the common gas return line allow us to work in a more stable condition up to 4 MV/m per cavity. With 250 mbar average pressure in the Cryostats, the pressure oscillation at 30 Hz frequency is reduced to 0.2 mbar amplitude correlated to a cavity phase oscillation of $\pm 5^{o}$, as shown in Fig. 18.

Table IX – Summary of operations attempt to optimise the Crystal–Refrigerator interaction.

OPERATION	EFFECT
Shut down of all the Vacuum Pumps	None
Shut down of Turbines	None
Shut down of Compressor	None
Variations of LHe level in the Cryostats	None
Increasing of thermal load switching on heater resistor in LHe tank up to 30 W per Cryostat	LHe level and average pressure more stable but no reduction of pressure fluctuations
Setting the Cryostat inlet valves in manual control at a constant opening in equilibrium with power dissipated	None
Setting the Cryostat inlet valves fully closed	Worst
Cooling of the LHe level probe tube, allowing cold gas flow through the closing flange in order to destroy hypothetical thermoacustic oscillations	None
Variations of LHe level in the Phase Separator Dewar	None
Variations of the pressure difference between Phase Separator Dewar and Cryostats	Better when the DP is lower (around 150 mbar)
Shut down of the heater in the Phase Separator Dewar	None
Setting all the Refrigerator valves in manual control at a constant opening in equilibrium with power dissipated	None
Increasing pressure in the Return line	**Strong reduction of the oscillation when average pressure in the Cryostats exceeds 200 mbar**
Decoupling of the Cryostats from the common gas return line closing to 50% the gas return valve	**Reduction of pressure oscillations in all Cryostats**

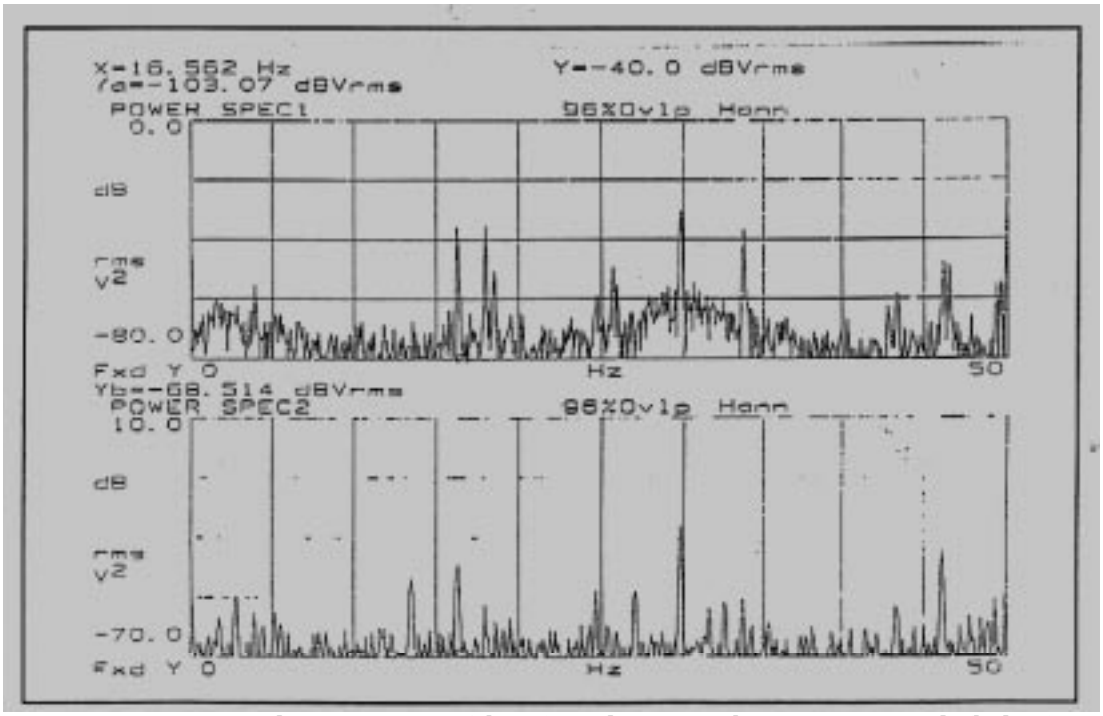

Figure 18 – Helium pressure (above) and cavity phase error signal (below) spectra. Average bath pressure 250 mbar, it shows the same peaks as Fig. 17 at 33 Hz frequency but with a pressure oscillation amplitude of 0.2 mbar (above) correlated to a cavity phase oscillation of $\pm 5^{o}$ (below)

9 – Beam Diagnostics

Intercepting and non intercepting diagnostics are widely used on LISA both for helping in beam transport and for beam parameter measurements.

Intercepting diagnostics consists in fluorescent screens and Optical Transition Radiation (OTR) reflecting mirrors mounted on a vertically moving vacuum feedthrough. Up to two square screens of 5 cm side can be mounted on the same holder. Chromium doped allumina screens have a very high light emission efficiency, and are used all along the linac to monitor beam transport. Each screen is seen by a standard CCD camera, whose output, through a video multiplexer, goes to a frame grabber which is a part of the Control System. A video output from the frame grabber is sent to a TV monitor; in this way the operator has a continuos vision of the beam, while on the Control System console it is possible to have quantitative information derived by the digitized images. Typically beam center position and second order momentum in horizontal and vertical planes are graphically displayed. These values can also be used by other tools of the Control System such as raster scan of the beam or magnetic lens strength variation for emittance measurement. If required, the last digitized image can be frozen on the monitor or stored for off–line analysis.

The efficiency of these fluorescent screens, on the other hand, is a limitation for a high charge per pulse accelerator as in our case, giving rise to saturation and in general to an overestimation of the beam spot size. In the low energy part of the injector (100 kV) in which a high current up to 200 mA is transported with macropulse length of the order of 1 ms, charge pile–up on the screen prevents even the simple observation of the beam spot [14]. Bulk aluminum screens with thick surface anodization were then added in this accelerator section.

The light yield of pure aluminum oxide is much lower, but enough to give clear images of beam position and dimensions. We have not performed systematic analysis of linearity and resolution of this kind of screens, and we never used them for quantitative measurements

At the time of the start of LISA commissioning, the possibility of a practical use of OTR for electron beam diagnostics had been demonstrated by Rule and Fiorito [15] using high peak current linacs designed for FEL applications. In our case the rather low charge per pulse was more than compensated by the long macropulse, so we decided to insert also a metallic mirror for more accurate measurement of beam parameters using OTR.

After initial difficulties caused by strong x–rays noise, fluorescence background due to stray electrons hitting the aluminum vacuum pipe and wide aperture of emitted radiation, we succeeded to observe OTR even at the injector energy of 1 MeV and using a standard CCD camera. With the improvement in transport efficiency, it was then possible to use OTR after the 180˚ bending arc for emittance measurement [16]. Beam spot image resolution resulted better than that obtained with fluorescent screens.

After the SC linac, with a beam energy of 20 MeV and 0.5 mA current, OTR was easily seen due to the more favorable angular distribution. At the beginning a strong fluorescence background produced by the dark current from SC cavities and dispersed on the pipe by the quadrupoles prevented a clear measurement, but when the dark current was strongly reduced working at a lower energy to stabilize the accelerating field, quantitative measurements of beam dimension were possible, and OTR screens are now currently used.

Figures [19] and [20] show a typical beam image, after a simple filtering to eliminate the "salt and pepper" noise, and the corresponding horizontal beam profile.

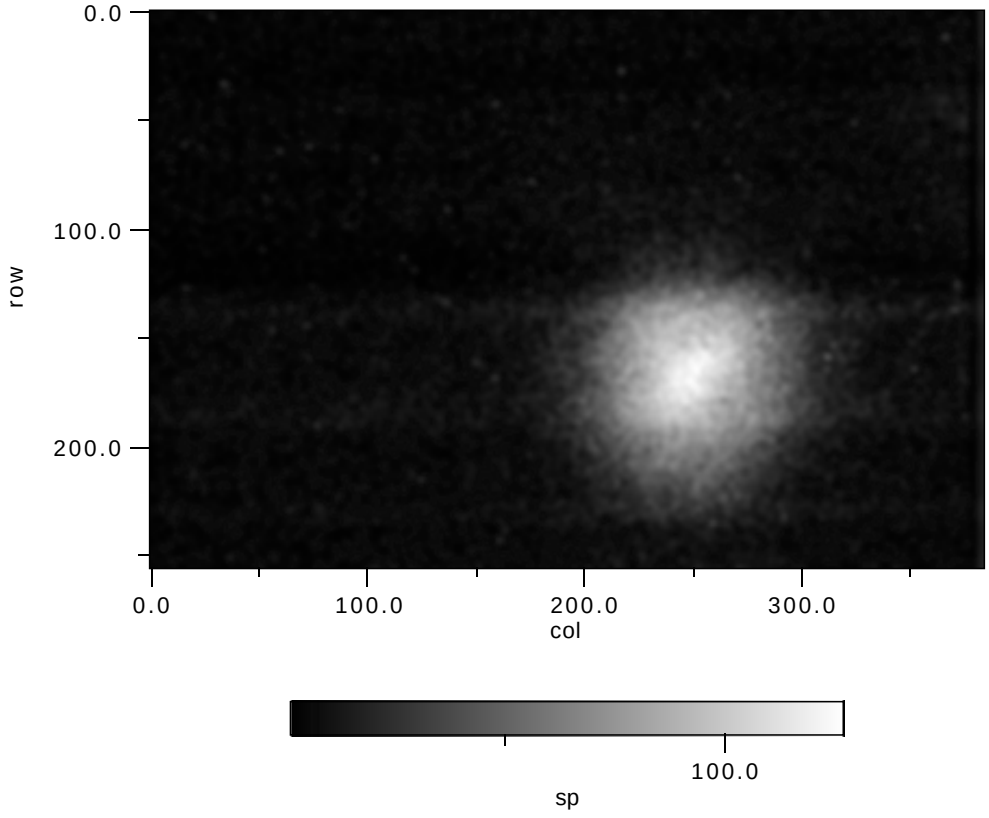

Figure 19 – OTR image of the LISA beam.

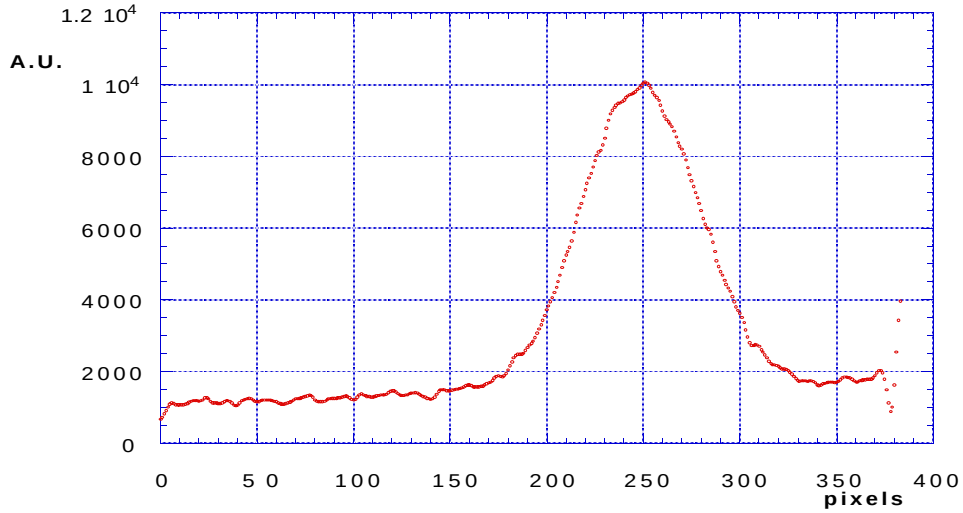

Figure 20 – Horizontal beam profile from previous image.

Beam current is measured by means of Faraday cups in two beam dumps, after the capture section and in the high energy spectrometer. Continuos beam current monitoring in different part of the accelerator is performed by a number of Pearson Electronics toroids (model 110A) which allow precise measurement of the average macropulse current. The toroid outputs (.1 V/A) are amplified by a factor 100 and sent both to a scope for direct visualization, and to an ADC for use inside the instruments of the Control System.

A non intercepting beam position monitor (BPM) system, based on quad stripline pick ups, is used in the lines following the 1 MeV capture section. The stripline length is ~15 cm. This length is ~1/10 of the optimal but impratical $\lambda/4$ length at 50 MHz. The signal amplitude is therefore just 0.15 of the maximum; The calculated sensitivity is 0.11 mV/(mA mm).

The transverse BPM size was limited by the diameter of the quadrupoles bore. The inner strips, at fixed distance from the external vessel and welded to it at the end opposite to the coaxial feedthrough, constitute a 50 Ohm short circuited transmission line. The size of the striplines realizing a characteristic impedance of 50 Ohm is very small and implies a tight mechanical tolerance. They have been machined from bulk aluminium since stainless steel proved unsuitable due to residual stress deformation after machining and welding.

The electronic detector for each BPM is composed of a couple (horizontal and vertical) of two matched narrowband channels followed by a differential amplitude to phase converter and an EXOR phase detector, providing an on line bipolar readout of the beam position independent of the beam current. The output is fed to a Sample & Hold, simultaneously triggered 16 channel ADC. The parallel channel signal handling instead of the simpler multiplexed channel, allows to get a snapshot of the beam trajectory.The output range is ± 1 V/cm, with a broadband noise of 5 mV_{rms}. This give a position resolution of ± 50 μm.

The matching between the channels of each couple can be impaired by thermal drifts,

causing an apparent beam displacement. To take care of this error a reference 50 MHz signal is injected in a calibration input whereafter it is equally splitted toward the four channels. At the input of the electronic chain a two–way selector can switch in the calibration or the beam signal, so that electronic drift offset, affecting both calibration and beam signal, can be subtracted to obtain the real beam position.

At the LISA nominal operating current of 2 mA BPM operation is reliable, but at lower current, as often in the commissioning of the arc, the response is less stable; since the useful signal amplitude is the 50 MHz component of the beam modulation, proper tuning of the inflector has had a crucial role for optimining the performances of BPM, and vice versa, allowing BPM operation at current as low as 0.5 mA. The direct signal from striplines, although these were not explicitly designed to provide high frequency response, was very useful in later stage to optimize the beam chopping, looking at the full spectrum from 50 to 2500 MHz [17].

In Fig. [21] we show two beam trajectories in the 1 MeV arc, obtained by making two distinct percentual variations of the fields of all the bending magnets. They are bumps with nodes at the extremities of the arc as expected from the achromaticity. They have been detected with the strip lines.

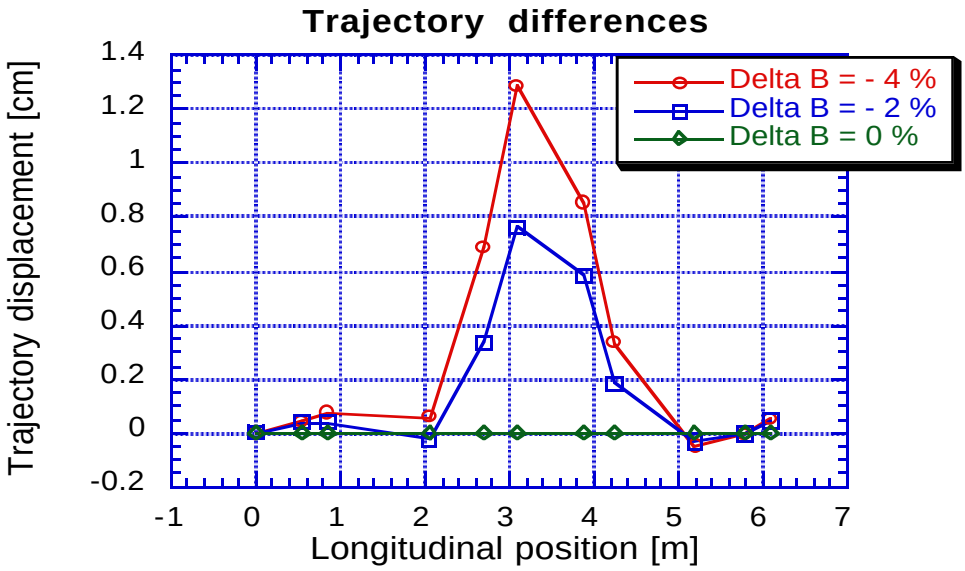

Figure 21 – BPM measurement of the relative beam displacement in the arc varying the bending field of –2% (square points) and –4% (dot points).

10 – Conclusions

The commissioning of LISA has been concluded with the limited forces of our small group (6 graduates and 3 technicians). We had moreover the support of external industries for maintenance and repairing of apparatus. This has been possible thanks to the high degree of automation of the whole machine and to the easy use of the Apple Mac Intosh man–machine interface. This experience should give confidence to those who are planning to istall such a kind of SC linac in a University or Research Labs environment that cannot afford a numerous team of specialized personnel.

On the other hand, a limited number of operators implies a careful organization of shifts in

order to keep the machine running for long periods, as it is necessary for an efficient use. In fact, as it takes about 3 days to cool–down the cavities and one day to warm–up and eventually a couple of days to recover the cold state in case of a transient elctrical energy failure, it is evident that running periods should be not less than one month. This can be achieved if an efficient automatic system of He gas recovery is provided, so that permanent presence of experienced personnel on the site is not required.

In our case we had not such a recovery system so that, unless the compressor was restarted by an operator in a few tens of minutes, the He gas was lost in air through the exhaust valves. This fact limited the running periods of LISA to about two weeks, which resulted in a very lengthy and unefficient commissioning.

The most difficult problem we encountered in commissioning, and which has ultimately limited the performance of the machine, was cavity vibrations due to thermo–acoustic oscillations in the refrigerator–cryostat system. This sort of problem is not peculiar of machines cooled at 4 K, as it is connected with the geometry of the structure. In Lisa it seems to be mainly due to the close interconnection of the gas circuits of the cryostats with common LHe and gas return lines from refrigerator to valve box. In fact a relevant reduction of vibrations has been achieved by closing partially the gas return lines from cryostats to valve box, thus decoupling somehow the citcuits. In other similar structures (JAERI–Japan) where each cryostat carries on top its small refrigerator, no such vibrations have been detected. A centralized scheme like ours is therefore not to be recommended. One should at least decouple each cryostat from the system by a local phase separator.

Two of the cavities show much stronger vibrations than the others.This may be due to some internal defect of insulation between the 4K body and the 70k shield. When ultimately we succeeded in limiting the vibrations of these cavities so that the corresponding frequency deviation was within the loaded bandwidth, it was evident that the the voltage and phase stabilizing systems have to work at their best in order to keep beam energy fluctuations below 1%. The phase feedback is the more critical as it has sometimes to cope with $\pm$ 45 degrees deviations. The corrections require a lot of power from the klystrons and ultimately impose a limit on the voltage obtainable from these two cavities and therefore on the maximum stable beam energy $\approx$ 15 MeV), which resulted well below the peak achieved energy (20 MeV).

All cavities show structure deformations and field unflatness (see Table VII) and Q degradation with respect to factory values (see Fig 10). This however has not been the ultimate energy limiting factor, as the pulsed regime (with several % duty cycle) is widely compatible with the cooling power of the refrigerator and quench has rarely happened only for gradients well above 5 MV/m.

After the original degradation following the installation on the accelerator, the cavities have suffered no apparent further deterioration even though their inner walls have been hit frequently by the beam and moreover no laminar flow clean air has been employed during the frequent disassembling operations on the vacuum chamber. This is to say that the machine has revealed to be much sturdier in handling than feared at first.

We must mention that a higher injection energy would increase the efficiency of capture and transport through the SC cavities. It would also be better to have the injector on axis with the cavities, because imperfections in the achromaticity of the arc entail injected beam position

fluctuatios.

In conclusion, the correction of the defects of two of the cavities would allow us to attain the design goals. It is the priority given to other projects that has stopped the work on this machine, which has, by the way, shown many potential uses besides the original FEL driver application. The intense, high quality beams of such a machine have allowed us to detect OTR radiation without difficulty and many more experiments have been proposed, ranging from the generation of neutron showers to testing of coherent inverse Compton scattering.

References

[1] – A. Aragona et al., Proc. of the European Particle Accelerator Conference–Roma 1988, 52, (1989).

[2] – U. Amaldi et al., Proc. of the European Particle Accelerator Conference–Roma 1988, 49, (1989).

[3] – SC Linear Accelerators– Discussion meeting – Frascati 1986.

[4] – Proc. 3rd Workshop on RF Superconductivity– Argonne 1988 p.81.

[5] – C. Biscari et al– An injector for LISA– LNF–88/08(R).

[6] – C. Biscari– Lisa capture section: simulation of particle dynamics–LNF–89/086(R).

[7] – A. Aragona, C. Biscari, R. Boni, M. Castellano, V. Chimenti, A. Gallo, S. Kulinski, C. Sanelli, B. Spataro, F. Tazzioli, F. Tian, M. Vescovi, Proc. of the 2nd European Particle Accelerator Conference – Nice. Editions Frontières 511 (1990).

[8] – M. Castellano, P. Patteri, F. Tazzioli, J. Zhuang, N. Cavallo, F. Cevenini, F Ciocci, G. Dattoli, A. Dipace, G.P. Gallerano, A. Renieri, E. Sabia, A Torre, Nucl. Instr. Meth. in Phys. Res. A318, 168 (1992).

[9] – A.Aragona et al., Proc. of 1988 Linac Accelerators Conference, Newport News, 632 (1989).

[10] – M. Castellano, S. Kulinski, P. Patteri, F. Tazzioli, M. Vescovi, N. Cavallo, F. Cevenini, Nucl. Instr. Meth. in Phys. Res. A332, 354 (1993).

[11] – M. Castellano, M. Ferrario, S. Kulinski, M. Minestrini, P. Patteri, F. Tazzioli, L. Catani, S. Tazzari, Nucl. Instr. Meth. in Phys. Res. A332, 347 (1993).

[12] – Tesla Test Facility Linac–Design report, Ed. D.A. Edwards– Desy print 95–01–1995.

[13] – A. Marziali and H.A. Schwettman, Tesla note 93–40.

[14] – M. Castellano et al.– The Diagnostics System for the SC Linac LISA, Proc. Firts European Workshop on Beam Diagnostics and Instrumentation for Particle Accelerators CERN PS/93–35 (BD) 176 (1993).

[15] – R. B. Fiorito, D. W. Rule, A. H. Lumpkin, R. B. Feldman, B. E. Carlsten, Nucl. Instr. Meth. in Phys. Res. A296, 739 (1990).

[16] – M. Castellano, L. Catani, P. Patteri, L. Gregorini, Proc. of 4th EPAC – London. Word Scientific 1670 (1994).

[17] – M. Castellano, M. Ferrario, M. Minestrini, P. Patteri, F. Tazzioli, L. Catani, S. Tazzari, G. Cavallari, Submitted to EPAC 96 – Barcelona – 1996.